A Population Balance Model of the Solution-Mediated Phase Transition of Citric Acid

Gilles Févotte
Université Lyon 1, LAGEP CNRS UMR 5007, Campus de La Doua. 43 bld. du 11 Novembre 1918, 69622 Villeurbanne Cedex, France
Ecole Nationale Supérieure des Mines de Saint Etienne, LPMG, CNRS UMR 5048, 158, cours Fauriel, 42023 Saint-Étienne, France

Caillet Alexandre and Sheibat Othman Nida
Université Lyon 1, LAGEP CNRS UMR 5007, Campus de La Doua. 43 bld. du 11 Novembre 1918, 69622 Villeurbanne Cedex, France

DOI 10.1002/aic.11261
Published online August 27, 2007 in Wiley InterScience (www.interscience.wiley.com).

The Solvent-Mediated Anhydrous to Monohydrate Phase Transition (SMPT) of citric acid in water was monitored using in situ Raman spectroscopy and image analysis. The solid phase composition, solute concentration, and crystal size distribution were measured during experiments designed to investigate the different steps of the SMPT process: dissolution of the metastable form, nucleation, and growth of the stable form. A Population Balance Model (PBE) was developed to depict the time evolutions of the two populations of particles involved. Nucleation and growth phenomena were analyzed and described through simplified kinetic laws. The related kinetic parameters were estimated through the nonlinear least squares minimization of model-experiments prediction errors. The overall PBE model was finally found to satisfactorily describe the SMTP process; the time variations of the solute concentration and solid phase composition in particular. It is clearly shown that the secondary nucleation of stable monohydrate particles depends on both the supersaturation and the overall solid content. Surprisingly, as far as the nucleation of stable particles in the presence of metastable solid is concerned, the rate of particle generation was found to exhibit identical dependency on the metastable and stable content, a feature which remains to be further investigated and explained. © 2007 American Institute of Chemical Engineers *AIChE J,* 53: 2578–2589, 2007

Keywords: crystallization, suspensions, nucleation, solid-state physics, simulation, process

Introduction

Even though it is clear that the parameters defining the equilibrium data of solid polymorphs and solvates are fixed by thermodynamics, it is well known that many industrial problems related to solid phase transition phenomena arise from the fact that most solute/solvent systems are likely to spontaneously remain far from their most stable state. Indeed, Ostwald's celebrated rule of stage[1] makes obtaining the most stable form rather uncertain: "... in the course of transformation of an unstable state into a stable one the system does not go directly to the most stable conformation but prefers to

Correspondence concerning this article should be addressed to G. Févotte at fevotte@lagep.cpe.fr.

reach intermediate stages having the closest free energy to the initial state." The rule of stage causes many problems as most properties of solid products (particles, tablets, powders, etc.) depend strongly on their solid state (i.e., amorphous vs. crystalline, anhydrous vs. hydrate or solvate, polymorphic state . . .).[2,3] As far as crystallization processes are concerned, particle features such as the Crystal Size Distribution (CSD), crystal habit, chemical purity, ease of downstream processing (e.g. filterability, behavior on storage, flowability), therapeutic efficacy, etc., depend on the solid state, and this is the reason why it is a major industrial issue to analyze and understand the fundamental phenomena governing the occurrence of phase transition processes.

As a major consequence of Ostwald's rule of stages, transitions between metastable forms and more stable ones are likely to occur at any time and for many possible reasons during the industrial processing of solid crystallized products.[3–5] Solid phase transitions are also governed by kinetic aspects which until today were rather seldom described in the literature. It is however obviously essential to understand how phase transitions take place during industrial solids elaboration and processing operations. The main reason for the little number of publications focused on the dynamics of phase transition phenomena arises from the lack of in situ sensors enabling the solid state to be quantitatively monitored in-line. Many analytical techniques are being currently used to characterize the solid form,[3,6,7] but most of these techniques are unsuitable for the in-line monitoring of industrial processes. Moreover, withdrawing and off-line analyzing crystallizing suspensions is extremely difficult to perform and requires many precautions to be taken since one deal with unstable samples. This is the main reason why, as they can be performed in situ, raising process vibrational spectroscopic technologies offers promising means of monitoring phase transformation phenomena during industrial solids elaboration processes. The Food and Drug Administration's PAT initiative[8] is a significant illustration of hopes which were put in the development of innovative sensing techniques. Among these techniques, Raman spectroscopy appeared in the past recent years as "one of the fastest, most reliable and most suitable techniques to identify crystals forms in drug products and can be easily exploited routinely for monitoring phase changes in drug products and quality control assays."[9]

During solids elaboration or processing, the presence of liquid phase often promotes the occurrence of phase transition phenomena. This is why solvent-mediated phase transitions (SMPT) were reported to take place during particulate processes and, in particular, during suspension crystallization processes. The basic phenomena involved during SMPT were early described by Cardew and Davey.[10] Figure 1 shows a schematic of a typical solute concentration trajectory during SMPT processes. According to Ostwald's rule of stages, the crystallization starts through seeding or primary nucleation of the metastable Form I, the initial concentration being C^*_{initial}. The concentration decreases during Phase 1, as the metastable particles grow. After reaching Point 2 the concentration C_S crosses the solubility curve of Form I (C^*_I) due to the nucleation and growth of Form II. Form II remains supersaturated while Form I becomes undersaturated. C_S goes on decreasing and usually reaches a plateau, due to the competition between nucleation and growth of Form II, together with

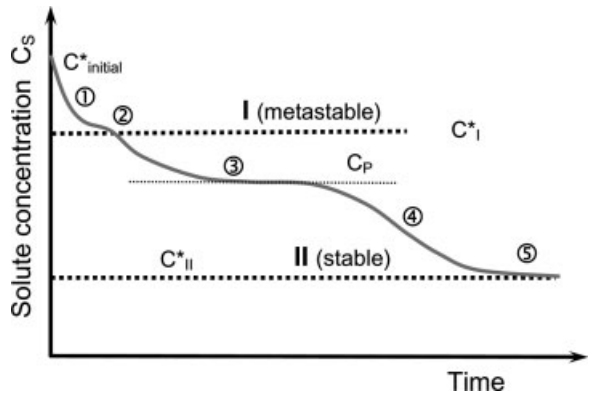

Figure 1. Schematic representation of the concentration versus time plot during the solvent-mediated solid phase transition of a dimorphic system in suspension.

the dissolution of Form I. The "pseudo steady-state" concentration value around Point 3, denoted by C_P in Figure 1, therefore results from the relative rates of the main crystallization and dissolution phenomena occurring between C^*_I and C^*_{II}. After full dissolution of the metastable particles (during period n°4), C_S is allowed to decrease until the system reaches the solubility of the stable form (period no. 5). Therefore, it is clear that the basic mechanisms involved during the SMTP process do not differ from "usual" crystallization phenomena: primary and secondary nucleation of stable and metastable forms, crystal growth, and dissolution of the metastable particles. However, as outlined below, the nucleation mechanism(s) of the stable form in the presence of metastable particles is (are) not always well understood, and it is one of the main issues of the present paper to investigate more clearly how nucleation of the stable form occurs, and which relevant kinetic equations can be applied to describe the generation of stable forms in the presence of metastable solids.

As far as complex multiphase systems are concerned, several articles have reported on the use of *ex situ* Raman spectroscopy for monitoring purposes. It should be noticed that *in situ* application are more seldom, as outlined in the sequel.[11–22] These papers describe calibration procedures enabling the in situ measurement of the polymorphic or "pseudo-polymorphic" composition of particles in suspension, and present in-line data on the time variations of the solid phase composition during phase transition experiments. The possibility of acquiring such dynamic data is invaluable to analyze, understand, and design mathematical kinetic models for phase transition phenomena.

During the present study, the transition of citric acid from the anhydrous to the monohydrate state was selected as a model system. The solid composition and the overall solid concentration were measured using Raman spectroscopy,[21] while the time variation of the CSD of citric acid particles was assessed through in situ image acquisition.[22] Following these experiments, a dynamic Population Balance Equation (PBE) model was designed and reported[23] to describe the isothermal seeded crystallization of pure monohydrate Citric Acid (mCA is the stable form at 15°C). The kinetic parameters involved by secondary nucleation and growth of mCA,

and by the dissolution of the anhydrous form, were estimated after fitting a set of experimental data to the PBE model-predictions. These experimental and modeling results were a requisite for the investigation of the whole phase transition process involving the dissolution of anhydrous metastable citric acid particles followed by the nucleation and growth of monohydrate, at 15°C. A priori, designing separate kinetic models for the different phenomena summarized in Figure 1 is not a sufficient condition to satisfactorily describe the whole anhydrous to monohydrate phase transition process: secondary nucleation of the stable form is likely to take place in the presence of high anhydrous solid content according to specific mechanisms which may not be observed during the crystallization of the sole monohydrate. It is therefore the aim of this paper to present an overall kinetic model describing the SMPT process in question. In particular, the rate of monohydrate secondary nucleation in the presence of anhydrous crystals was evaluated. To the best of our knowledge, only two studies dealing with the kinetic PBE modeling of SMPT processes were reported in the literature.

Ono et al.[12] presented a PBE simulation model for the SMPT of L-Glutamic acid from the α-form to the stable β-form. Dissolution rate of the metastable form and nucleation and growth rates of the stable form were represented using phenomenological models; No nucleation of new metastable crystals was assumed to take place. The dissolution of the α-form was assumed to be linearly dependent on the absolute undersaturation. The growth rate of stable form was also assumed to be first-order with respect to the absolute supersaturation, while a possible size-dependence of this rate was represented through the introduction of a multiplicative power function of the particle size. As in other reported experimental studies, the secondary nucleation rate of the stable β-form, $R_{n_{2\beta}}$, was assumed to be proportional to the concentration of stable crystals generated in suspension. The kinetic parameters for the dissolution of the metastable form and for the nucleation and growth of the stable form were estimated through the minimization of a cost function computed using Raman measurements of the solute concentration and solid phase composition and discrete-time CSD measured using laser diffraction technique. The initial CSD of the two polymorphs was assumed to be described by a combination of three log-normal distributions. New crystals generated during the process were found to result from a rather complex combination of primary and secondary nucleation mechanisms. The model finally underlined some limitation of the overall kinetic process through the growth of the β-form. As a consequence of this latter kinetic feature, the various nucleation phenomena involved during the SMPT process could not be accurately assessed due to the lack of sensitivity of the overall experimental behavior to nonlimiting nucleation phenomena. Even though significant new experimental and theoretical information was brought by Ono et al.,[12] it turned out that investigating the nucleation mechanisms governing the SMPT processes remains a difficult, yet important task.

One of the very few PBE modeling study which, to our knowledge, was published in the open literature was also devoted to the SMPT of L-glutamic acid.[15,19,20] In situ monitoring of the crystallization of the metastable form was performed using ATR-FTIR (Mid Infrared Attenuated Total Reflectance), Raman spectroscopy, PVM, and Focused Beam Reflectance Measurement (FBRM) probes. Specific experiments were carried out to estimate the kinetic parameters of primary and secondary nucleation rates of the metastable α-form[20] from induction time measurements. As in the previous study, CSD estimates were obtained off-line after suspension samples were withdrawn from the crystallizer during desupersaturation experiments; a coulter counter (electro-sensing zone counter) was used for this purpose. Interestingly, during unseeded experiments it was observed that the level of initial supersaturation had no effect on the transformation time, a rather paradoxical dynamic feature of the process which was attributed to complex counteracting effects. This feature was further satisfactorily described by the model of the SMPT process and kinetic parameters were estimated in order the model predictions to fit the experimental data (i.e., the evolutions of the solute concentration, solid polymorphic composition, and final average particle size). The growth rate of metastable crystals was expressed through the "Birth and Spread" model and diffusive limitations were taken into account. Both unseeded and seeded SMPT experiments were then carried out in order to investigate the $\alpha \rightarrow \beta$ phase transition process. As displayed in Figure 2, in situ image acquisition revealed surface nucleation of the stable β-form on α crystals. Consequently, the nucleation of stable β crystals was assumed to result from both heterogeneous and surface nucleation mechanisms, the latter phenomenon being proportional to the specific surface of the α crystals (i.e., the second moment of the CSD), a feature that was not clearly observed by Ono et al.[12] As Figure 2 shows, the estimated kinetic parameters of the two secondary nucleation mechanisms are such that heterogeneous nucleation does not play any role in the generation of new stable particles: for a supersaturation degree of 2, about 1.7×10^9 particles are generated per sec-

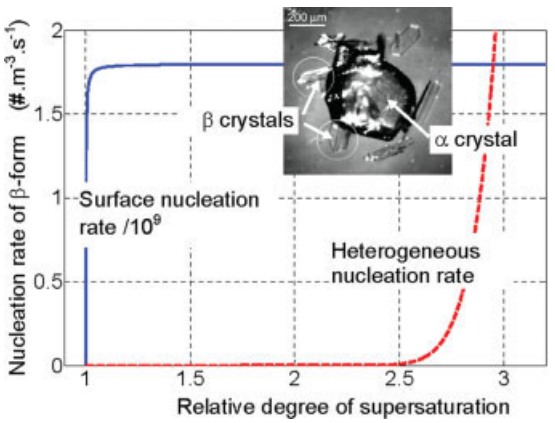

Figure 2. Respective contributions of surface and heterogeneous mechanisms to the secondary nucleation rate of the β-form of Glutamic acid as a function of the relative degree of supersaturation.

Calculation based on the kinetic parameters estimated by Schöll.[20] The α-CSD distribution corresponds to spherical particles of 200 μm, the selected range of supersaturation corresponds to the experiments performed. Inset: in situ PVM image of the surface nucleation of β-form on the surface of metastable α crystals (after Schöll[20]). [Color figure can be viewed in the online issue, which is available at www.interscience.wiley.com.]

ond and cubic meter through surface nucleation while the number of particles issued from heterogeneous nucleation is not significant. Surface nucleation of β on α crystals dominates the generation of stable crystal during the SMPT process.

In a different field of application, kinetic and PBE modeling studies were devoted to the preferential crystallization of enantiomers.[24] As in situ sensors, Elsner et al.[25] use in-line polarimetry and densimetry to monitor the batch crystallization of DL-threonine in water. Combining these two measurements allows the authors to compute the time variations of the overall solid concentration and of the weight fractions of the two enantiomers. A dynamic model of the crystallization was developed using the method of moments which, for the estimation of nucleation and growth parameters, required experimental data about the CSD variations. Information about the distribution of surface area (i.e., the second moment of the distribution) was achieved using optical microscopy. The obtained PBE model was finally shown to capture the main features of the crystallization process, even though imperfect prediction of the nucleation rates was reported.

On the subject of the present study, the aforementioned experimental and modeling works dealing with the crystallization of glutamic acid and threonine allow one to outline the following points:

- The joint use of several in situ sensors for the investigation of complex crystallization systems, Raman spectroscopy in particular, is very infrequent even though it provides highly valuable experimental data.
- Compared with overall standard kinetic models, PBEs allows a much deeper analysis and understanding of the basic phenomena occurring during crystallization processes. In particular, as they aim at reproducing the "history" of the different particles generated all along the crystallization process, PBEs appear as a privileged means of understanding and evaluating nucleation phenomena governing the SMPT.
- As far as SMPT processes are concerned, it is an important result to understand and evaluate to which extent surface nucleation of stable particles on metastable ones initiates the generation of stable crystals in suspension.

Bearing the aforementioned literature data in mind, the aim of the present paper is twofold:

- A synthesis of our previously published results about the crystallization of citric acid monohydrate[21–23] is made to extend the application of these results to the modeling of the whole SMPT of citric acid. New experiments are presented later, during which seeded anhydrous to monohydrate phase transition of citric acid were monitored using Raman spectroscopy and image analysis.
- During the development of an overall PBE model describing the SMPT of citric acid, original results were obtained about the secondary nucleation of the stable phase. Results of the kinetic parameter estimation performed to fit the overall PBE model, which are also presented later, bring answers to some of the questions raised by the two aforementioned studies.

As far as secondary nucleation of a stable solid phase in the presence of a metastable one is concerned, Davey et al.[26,27] investigated the SMPT of 2,6-dihydroxybenzoic acid (DHB) in toluene and chloroform with varying temperature and initial concentration. Discrete-time estimates of the solute concentration were performed through UV/vis absorption measurements at 327 nm, allowing the main dynamic features of the time-variations of the process to be assessed. Nucleation of the stable Form II was thus demonstrated to be the limiting kinetic step.

The ability of metastable α L-glutamic acid crystals to nucleate the stable β polymorph was examined[28,29] using optical microscopy and XRD. It appeared that the nucleation of β crystals was promoted by the presence of α seed particles. Moreover, it was concluded that the induction of β nucleation by α surfaces should be "catalyzed" by the attrition or breakage of particles during the development of the crystallization process. Ferrari et al.[30] studied the α to β phase transition of glycine in hydro-alcoholic solvents. Because of the many simultaneous phenomena involved during the process, complex and rather paradoxical effects were described. For example, with varying ethanol concentrations, it was observed that despite increasing initial supersaturation levels, the rate of transformation was decreased. Such effect was finally explained by the control of the SMPT process through the dissolution of the metastable form.

Experimental Design

For the sake of readability, some aspects of the experimental strategy are recalled here, but detailed information can be found in previous papers.[21,22] The anhydrous/monohydrate (aCA/mCA) SMPT of Citric acid in water was investigated as a model system. The solubility of citric acid is of the order of 1.5 kg/kg water at 20°C. The solute/solvent system exhibits an enantiotropic-like behavior with a transition point located near 34°C. Experimental data about the solubility diagram of citric acid in water were reported by Groen and Roberts.[31] Isothermal desupersaturation experiments were performed at 15°C where anhydrous CA is metastable. Monohydrate and anhydrous forms were purchased from Acros Organics (Citric acid anhydrous, Reagent ACS, 99.5% and monohydrate p.a.) and used in distilled water without further purification.

Figure 3 shows a schematic representation of the lab-scale crystallization equipment used in this study. For satisfactory Raman monitoring of the solid state, the 2.5-L glass reactor was insulated from light and equipped with a jacket and a

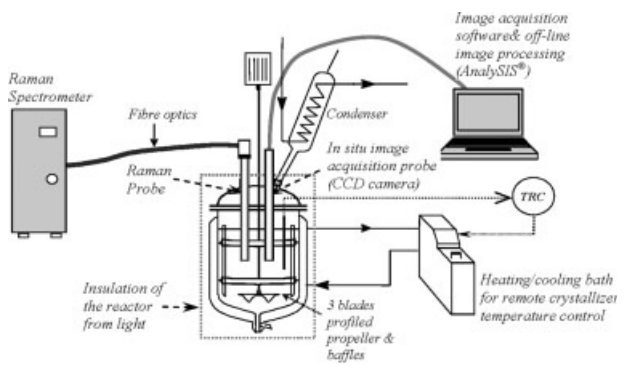

Figure 3. Schematic of the 2.5-L isothermal crystallizer equipped with an in situ Raman acquisition probe and immersed video CCD image acquisition system.

Table 1. Isothermal (15°C) Seeded aCA to mCA Phase Transition Experiments: Main Operating Conditions

	Initial Mass of Crystallized aCA Particles, wt %	Mass of mCA Seed Introduced in the Crystallizer, g	mCA Seed Amount, wt % of the Final Crystallized Mass of mCA	Preparation of the Seed
Run 8	6.0	0.12	0.02	Slurry
Run 9	6.2	1.03	0.22	Slurry
Run 10	6.5	9.89	2.15	Slurry
Run 11	6.4	1.07	0.23	Dry
Run 12	6.8	10.14	2.14	Dry

condenser. Stainless-steel baffles were used in conjunction with a speed-controlled stirrer; the stirring rate was set to 415 rpm and kept constant.

In situ measurements were performed using a ReactRA Raman spectrometer manufactured by Mettler–Toledo, equipped with a 16-mm-diameter immersion Hastelloy probe. The calibration of the Raman spectral measurements was presented elsewhere.[21] The calibration model allowed in-line monitoring of the solid composition (i.e., the ratio aCA vs. mCA) and of the overall solid concentration in the slurry. The absolute uncertainty of the overall solid composition measurement was found to be of the order of 3%, for measurements performed in the range 0–25 wt %, while it was found to be about 10% for solid composition measured between 0 and 100 wt % aCA. Complete information about the solid phase (i.e., partial and overall solid concentration) was obtained in real time using the dual-purpose calibration model. Such calibration approach turned out to be a very significant advantage of the technique since the computation of the overall CA mass balance allowed estimating reliable solute concentration data, even though the dissolved CA concentration was not directly measured. The solute concentration was expressed on the basis of anhydrous content. Two definitions of supersaturation were used:

$$\beta(t) = \frac{C(t)}{C^*(T(t))} = \frac{C(t)}{C^*} \tag{1}$$

$$\sigma(t) = \frac{C(t) - C^*}{C^*} \tag{2}$$

where C^* is the solubility and C the estimated solute concentration expressed in % (100 kg anhydrous basis solid/kg water.)

The dispersed solid phase was monitored using in situ image acquisition, followed by off-line image analysis. Pictures of the suspension were taken using an immersed CCD camera probe[22] as represented in Figure 3. Because of the difficulty of discriminating between individual particles at high solids content, the quantitative use of the video probe was restricted to the very first minutes of the crystallization process. During these early periods of the crystallization process, particle sizes were evaluated as the diameter of the equivalent ideal spherical particle with same projected area using analySIS®, an image processing software developed by Soft Imaging System.[22]

During the previously reported studies,[22–23] the experimental design was focused on investigating the nucleation and growth kinetics of monohydrate citric acid, the stable form at 15°C. Seeding was performed to avoid primary nucleation, on the one hand, and to ensure improved experimental reproducibility, on the other hand. For the present study, Runs 8–10 were carried out with almost constant initial solid content. About 6 wt % aCA slurries were obtained from seeded isothermal crystallization of aCA, as explained in Table 1. The operating conditions for these "standard" crystallization operations were described in more details by Caillet et al.[22] After reaching the solubility of the metastable form at 15°C the suspension was left under stirring for at least 24 h, to make sure that no spontaneous nucleation of the stable form occurred. Seed mCA particles were then introduced in the crystallizer to initiate the SMPT process. The stable seed particles were prepared as follows: stirred temperature-controlled slurries of seed crystals were prepared from sieved monohydrate particles; the class of size was selected to be 250–315 μm. To "activate" the seed crystals through partial surface dissolution, about 3% of the solid mass was dissolved prior to its introduction in the reactor.

Five typical phase transition experiments were selected for the present study. As displayed in Table 1, Runs 8–10 were carried out with almost constant initial aCA content and varying amounts of mCA seeds. Runs 11 and 12 were performed to investigate the effect of the seed preparation of the kinetics of the SMPT process. Indeed, as displayed in Table 1, these latter two runs were performed with the same operating conditions as Runs 9 and 10, respectively, except that dry seed was used.

Experimental Results and Discussion

Figures 4 and 5 display the time variations of the measured solute concentration and solid composition during Experiments 8–10. The overall rate of the SMPT process appears to be independent of the amount of seeds, a paradoxical phenomenon if one considers usual "basic" crystallization processes where increasing the mass of seed is expected to reduce the overall crystallization time. Concerning Run 10 in Figure 5, the rate of turnover appears to be slightly increased by the high seed amount. It should however be outlined that this observation does not mean that the overall transition rate increases. Indeed, the weight of seed stable particles cannot be neglected with respect to the initial amount of metastable solid during Run 10 so that the measured solid composition is shifted at the beginning of the experiment, but one can still consider that the rate of SMPT is identical to the overall rate during Runs 8 and 9.

Secondary surface nucleation of mCA was previously found to strongly depend on surface mechanisms,[23] a feature which was also demonstrated by Caillet et al.[19] and Schöll[20] about glutamic acid. One could therefore expect increasing surfaces of mCA crystals to promote the nucleation process, except if the growth rate of mCA was strongly rate-limiting. The latter assumption was contradicted by our previous

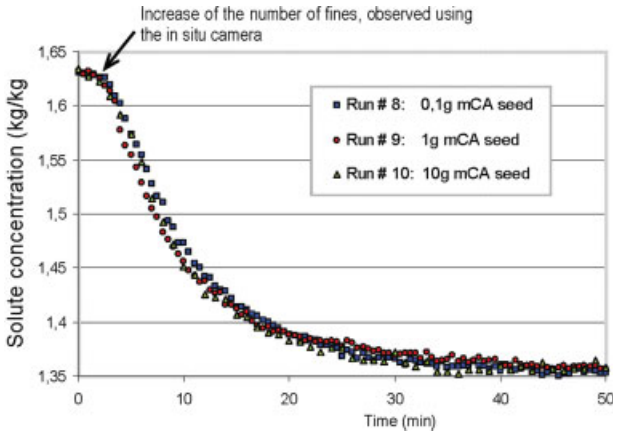

Figure 4. Runs 8–10: Solute concentration profiles measured using in situ Raman spectroscopy during three isothermal SMPT process performed with varying mCA seed amounts and constant initial metastable solid concentration (≈6 wt %).

[Color figure can be viewed in the online issue, which is available at www.interscience.wiley.com.]

experimental study of the crystallization of mCA.[23] It is therefore important for the model developed here to relate and explain the nondependency of the rate of turnover with respect to the amount of mCA seed crystals and it is reasonable to assume that the main difference between the kinetics of seeded mCA crystallization and the SMPT process lies in the involved nucleation phenomena.

To analyze the kinetic features of secondary nucleation, Figure 6 compares the concentration profiles obtained during Runs 3 and 9. Run 3 was performed with an initial supersaturation level similar to Run 9, and with the same stable seed amount (about 1 g), but no metastable suspension was initially loaded in the crystallizer. Run 3 was therefore a

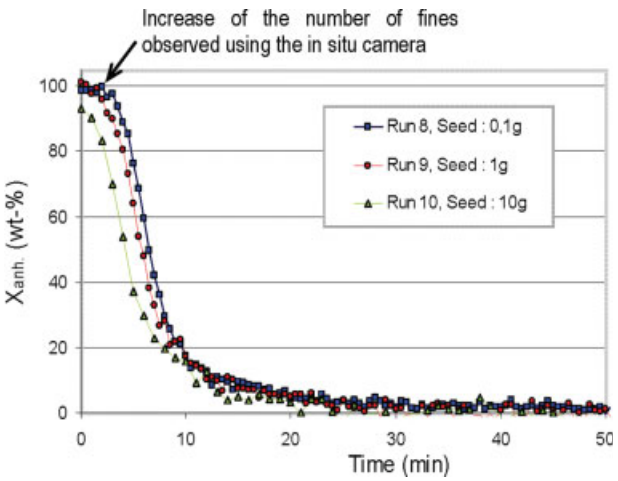

Figure 5. Runs 8–10: Solid composition profiles measured using in situ Raman spectroscopy.

X_{anh} is the anhydrous weight concentration in solid phase in %. [Color figure can be viewed in the online issue, which is available at www.interscience.wiley.com.]

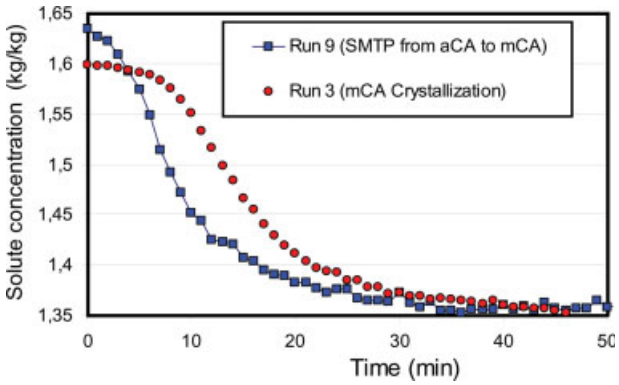

Figure 6. Comparative study between the overall mCA crystallization rates with and without the presence of anhydrous metastable phase.

Solute concentration profiles measured during isothermal Run 3 (batch seeded crystallization operation of mCA) and Run 9 (aCA to mCA SMPT operation), both performed with same mCA seed mass and similar initial supersaturation. [Color figure can be viewed in the online issue, which is available at www.interscience.wiley.com.]

"simple" seeded isothermal desupersaturation crystallization experiment. Surprisingly again, it is very clear that the overall rate of turnover is much higher during the SMPT process, despite the additional dissolution step involved. Consequently, two major differences can be outlined between stable crystallization operations and SMPT experiments: the amount of seeds has no more effect on the rate of turnover, and the overall stable crystallization rate turns out to be increased during phase transition operations. This in turns implies that the secondary nucleation mechanism(s) is (are) promoted during the SMPT process. It is then rather logical to assume that the presence of anhydrous crystals promotes contact secondary nucleation through interparticles collisions. Anyway, as no spontaneous nucleation of the stable form was observed in metastable suspensions, only anhydrous/monohydrate impacts would initiate this latter process. As outlined earlier, several studies have shown prominently that the stable form is likely to nucleate on the surface of the metastable particles.

With the aim of understanding the nucleation of the stable form, Figure 7 displays a comparison between pictures taken during Runs 3 and 9. From a qualitative point of view, even though Run 9 starts with a significant aCA solid content that makes the comparison difficult, it is rather clear that secondary nucleation (i.e., the generation of new small particles) is enhanced by the aCA crystals already in suspension. Rough estimates of the CSD were computed after analyzing the pictures in Figure 7. As displayed in Figure 8, during the first minute following seeding of the stable form, no significant increase of the number of fine particles was observed. Meanwhile, slight increase of the number fraction of big particles was measured, which can be attributed to the growth of crystals already in suspension. After 2 min, the fraction of smaller particles increased very rapidly. The time at which the appearance of new particles was noted corresponds to the increase of both rates of solute consumption and of anhydrous to monohydrate turnover, as indicated in Figures 5 and 6. From these observations and similar measurements made

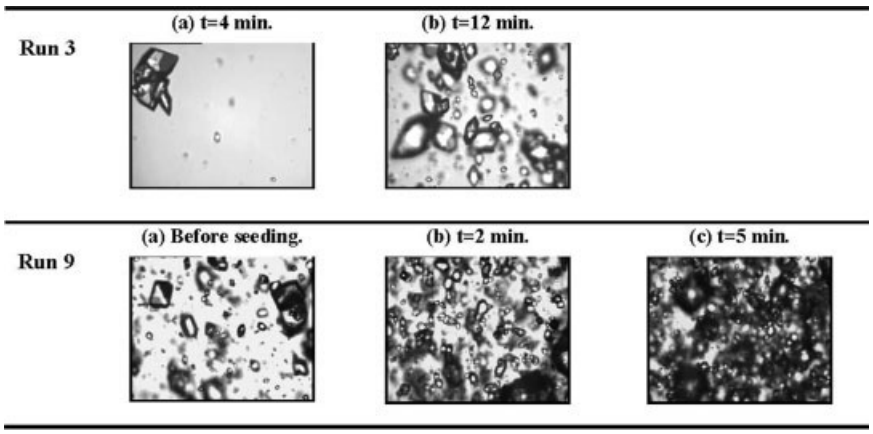

Figure 7. Pictures of the crystallizing suspension during Run 3 (seeded batch isothermal crystallization of mCA) and Run 9 (seeded aCA → mCA SMPT).

Both experiments were performed with similar initial supersaturation ($\Delta C_{monoh} \approx 0.35$ kg/kg) and mCA seed amounts (≈1 g).

after Run 3, it can be concluded that secondary nucleation of mCA indeed occurred earlier, and more intensely when solid metastable crystals were already in suspension.

As explained earlier (see Table 1), additional SMPT experiments were also performed with dry seed in order to study the effect of the seed preparation on the rate of turnover and, if possible, to get additional information about the secondary nucleation process of mCA in the presence of aCA particles. Even though different mechanisms are expected to take place after dry seed was introduced in the crystallizer (e.g., "false" nucleation due to the presence of tiny attrition fragments stuck on the sieved seed particles), both the experimental rates of solute consumption and of phase transformation turned out to be unchanged by the seed preparation. Figure 9 shows that the four concentration profiles measured during Runs 9–12 are identical to the best of the accuracy of the Raman measurements. The same observation can be made from the solid composition profiles, which are not reproduced here. Again, these experimental results plead in favor of dominating surface secondary nucleation mechanisms that would not depend on the surface properties of the metastable seeds, even though the mechanism in question was shown to depend on the amount of metastable suspension present at the beginning of the SMPT process.

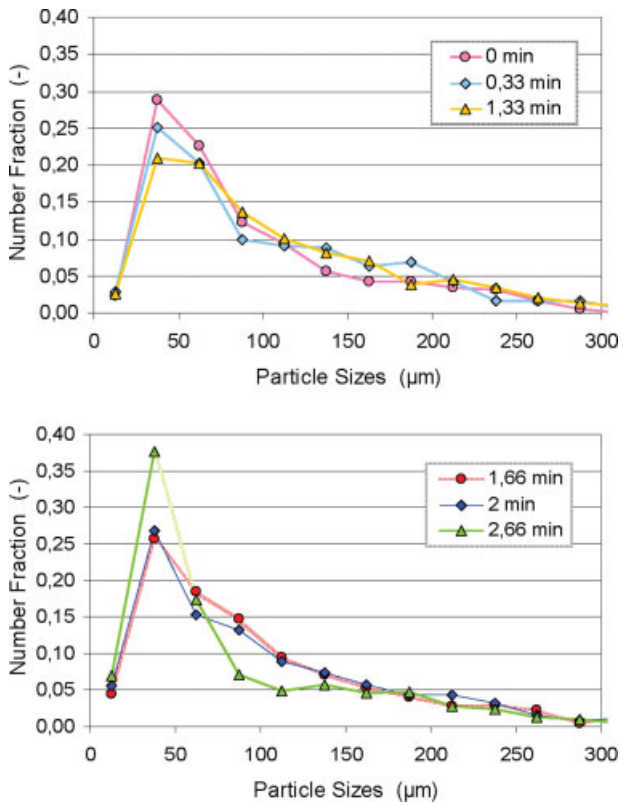

Figure 8. Run 9: Estimated evolutions of the number-CSD, measured using image analysis, during the first moments following the introduction of stable seed in the suspension.

[Color figure can be viewed in the online issue, which is available at www.interscience.wiley.com.]

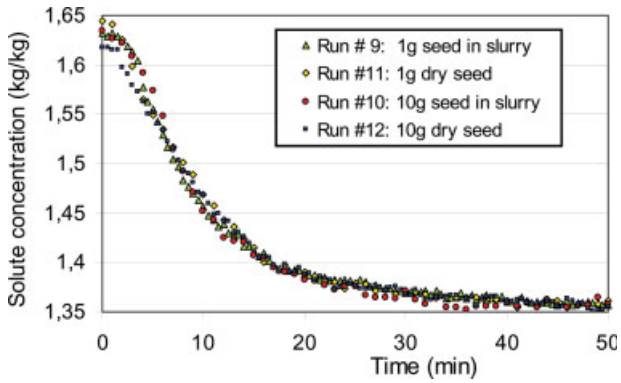

Figure 9. Demonstration of the invariability of the overall rate of phase aCA to mCA transformation despite changes in the amount and preparation of the stable mCA seed particles.

[Color figure can be viewed in the online issue, which is available at www.interscience.wiley.com.]

Table 2. Differential Expressions Used for the PBEs of the Two Pseudo Polymorphic Form, with Initial and Boundary Conditions

	Metastable aCA Population	Stable mCA Population
Main PBEs	$\frac{\partial \Psi_a(D_a,t)}{\partial t} + \mathcal{D}_a(t)\frac{\partial \Psi_a(D_a,t)}{\partial D_a} = 0$ (4)	$\frac{\partial \Psi_m(D_m,t)}{\partial t} + G_m(t)\frac{\partial \Psi_m(D_m,t)}{\partial D_m} = 0$ (5)
Initial conditions	$\Psi_a(D_a,0) = \Psi_{a,seeds}$ (6)	$\Psi_m(D_m,0) = \Psi_{m,seeds}$ (7)
Boundary conditions		$\Psi_m(D_m^*,t) \approx \Psi_m(0,t) = \frac{R_{N_m}(t)}{G_m(t)}$ (8)
	$\Psi_a(\infty,t) = 0$ (9)	$\Psi_m(\infty,t) = 0$ (10)

Population Balance Modeling of the Phase Transition Process and Kinetic Identification

As a preliminary step for the modeling of the SMPT, a detailed model describing the crystallization of the stable monohydrate form was reported by Caillet et al.[23] The particle sizes were characterized as the diameter of the equivalent spherical particles with same projected area D_m computed from image analysis measurements. Now, let $\Psi_m(D_m,t)$ and $\Psi_a(D_a,t)$ be the number density functions (in Nb m^{-1} m^{-3}) of monohydrate and anhydrous crystals of equivalent size D_m and D_a at time t, respectively, the PBE[32] describing both stable and metastable particles can be written as presented in Table 2.

Actually, the PBEs in Table 2 are rather simplified and notably assume that no agglomeration or breakage of the particles take place during the SMPT experiments. The left-boundary conditions express the generation of new crystals through nucleation. To be stable and grow, it is well known that the nuclei should exhibit a size exceeding a critical size D_m^*, which was assumed to be negligible for the numerical resolution. Moreover, the growth rate G_m was assumed to be size-independent. The "infinite size" represents any limit size that cannot be reached by the growing crystals, which explains the right-boundary condition in Table 2. The initial mCA population number density function is the measured monohydrate seed CSD. The time variations of the anhydrous CSD are expressed through the second PBE in Table 2. Because of undersaturated conditions no crystal growth now takes place, and metastable crystals reaching the limit size 0 vanish through dissolution: to reproduce this feature the left-boundary condition was simply left undefined and negative growth rate (i.e., $\mathcal{D}_a(t) < 0$) was used to represent the dissolution process:

$$\mathcal{D}_a(t) = \frac{dD_a}{dt} \tag{3}$$

As already explained, the initial anhydrous population density function was measured before the introduction of mCA seed particles in the crystallizer, and after the crystallized aCA slurry was left under isothermal condition for at least 24 h. Figure 10A shows the size distribution of the anhydrous seed particles measured using image analysis, $\Psi_a(D_a,0)$, as defined in Table 2. The anhydrous and monohydrate solubility concentrations were assumed to be $C_m^* = 1.63$ kg solute/kg water and $C_m^* = 1.348$ kg solute/kg water, at 15°C, and the densities were set to 1545 and 1658 kg/m^3, respectively.

The PBEs were solved using the multiphysics software package Femlab®. Equations 4 and 5 were introduced in Femlab as "Classical PDEs, Coefficient form." Both stable and metastable particles were computed in two one-dimensional spaces between 0 and 1.6 mm, the number of elements was set to 120. Refining the mesh in the neighborhood of size zero or increasing the total number of elements did not really improve the simulation results. The time-dependent solver was tuned with absolute tolerance 10^{-4} and relative tolerance 10^{-3}. The direct stationary linear solver UMFPACK with general solution form (six eigenvalues) was used.

The rates of monohydrate crystal growth, G_m, and contact secondary nucleation, R_{Nm}, were assumed to be represented through the following phenomenological kinetic expressions (11–13). According to experimental observations, it seemed reasonable to consider secondary nucleation as an activated contact mechanism: the nucleation rate in question appeared to be supersaturation-dependent and promoted by the concentration C_S of solid already present in suspension.[22] Figure 10B shows the size distribution of the seed monohydrate particles measured using image analysis, $\Psi_m(D_m,0)$ (see Table 2).

It should be outlined that the expression used to represent the secondary nucleation process does not account for the input stirring power. Such simplification was made possible because the stirring rate was set constant during all the experiments. However, it is clear that it would be useful to further improve our understanding of the nucleation process through a study of the effect of stirring on the secondary nucleation rate.

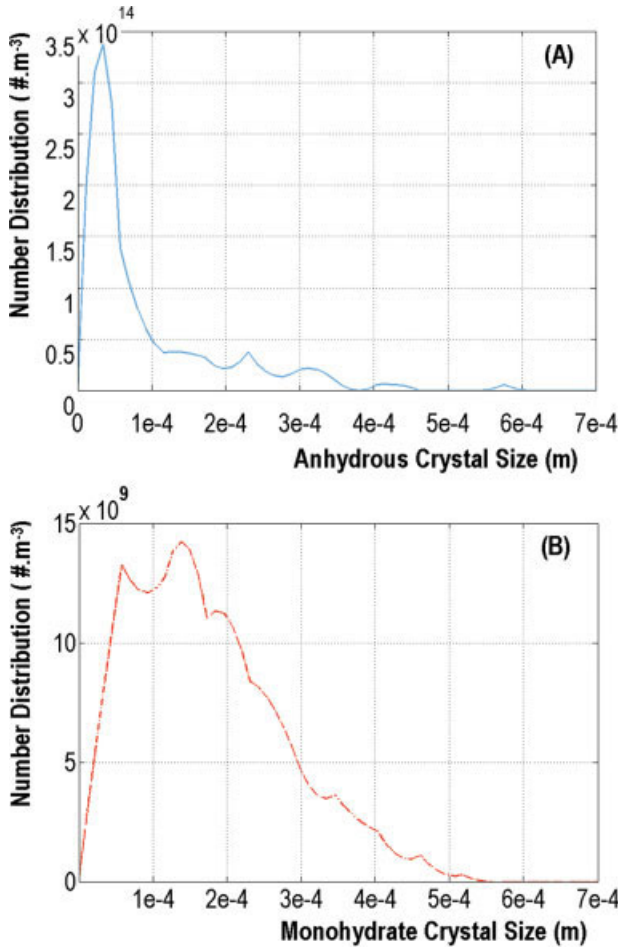

Figure 10. Number distribution of the seed particles measured using image analysis (interpolated from discrete size data): (A) Anhydrous, (B) Monohydrate.

[Color figure can be viewed in the online issue, which is available at www.interscience.wiley.com.]

$$\frac{dD_m}{dt} = G_m(t) = K_{gm}(C(t) - C_m^*)^{k_m} = 7.18 \times 10^{-6}(C(t) - C_m^*)^{1.58} \quad (11)$$

$$R_{N_{2m}}(t) = K_{2m}\, C_{S,m}(t)^{i_m}\, (C(t) - C_m^*)^{j_m} = 1.72 \times 10^{8} C_{S,m}(t)^{0.47}(C(t) - C_m^*)^{1.14} \quad (12)$$

$$\mathcal{D}_a(t) = \frac{dD_a}{dt} = K_d(C(t) - C_a^*)^{i_d} = 2.51 \times 10^{-6}(C(t) - C_a^*)^{1.07} \quad (13)$$

where $R_{N_{2m}}$ is the secondary nucleation rate of monohydrate citric acid (Nb s^{-1} m^{-3}); K_{gm} is the monohydrate growth rate constant (s/m); $C_{S,m}$ is the concentration of monohydrate crystals in suspension (kg/m^3), K_{2m} is a "lumped" kinetic constant for secondary nucleation of monohydrate; C_m^* is the solubility of monohydrate (kg Anh./kg water); k_m, i_m, and j_m are exponents related to monohydrate growth and secondary nucleation

The solute concentration $C(t)$ determines the level of supersaturation and consequently nucleation and growth events occurring in the crystallizer. $C(t)$ is required to solve the PBEs, but also results from the computation itself as any molecule appearing in the solid phase should be subtracted from the solute. Assuming known particle shape ϕ_p, the computed CSD allows one to calculate the mass of crystallized solid:

$$C_s(t) = \frac{\rho_m \phi_p}{M_m} \int_{L_0}^{L_{i,max}} \Psi(D_m, t) D_m^3 \, dD_m \quad (14)$$

with $\phi_p = \frac{\pi}{6}$ for spherical particles. ρ_m and M_m are the density and molecular weight of monohydrate crystals.

From the computed value of C_s, the solute mass balance provides the concentration of product remaining at the dissolved state, which can be compared to the measurements. The solute concentration was expressed in kg solute/kg solvent, and computed from the following mass balance equation:

$$C = \frac{\frac{C_T}{1+C_T} - \left(\left(1 - X_a(t)\right)\frac{M_a}{M_m} + X_a(t)\right)\tau_{sol}(t)}{\frac{1}{1+C_T} - \left(1 - X_a(t)\right)\left(1 - \frac{M_a}{M_m}\right)\tau_{sol}(t)} \quad (15)$$

where τ_{sol} is the anhydrous-basis solid concentration in suspension (kg solid/kg suspension); X_a is the anhydrous weight concentration in solid phase; C_T is the total solute concentration after full dissolution of the final solid (kg/kg water).

The many parameters involved in Eqs. 11–13 might allow to "artificially" match the simulation to the experimental data. This is why, in order to reinforce the credibility of the overall estimation procedure, three measures were taken:

1. Let θ be the vector of kinetic parameters required to quantify Eqs. 11 and 12:

$$\theta = [K_{gm}, K_{2m}, k_m, i_m, j_m] \quad (16)$$

As reported by Caillet et al.,[23] θ was estimated separately from specific isothermal seeded mCA crystallization experiments. A quadratic criterion Crit(θ) quantifying the mismatches between the simulated crystallization of mCA and the experimental data was minimized using "lsqnonlin," a nonlinear least squares Levenberg–Marquardt optimization routine available in Matlab® Optimization Toolbox. The PBE resolution program was used as a subroutine computing the model-predicted values of the measured process variables (i.e., the solute mCA concentration and some discrete-time estimates of the mCA CSD obtained through image analysis.)

2. Six mCA crystallization experiments were performed with varying operating conditions, and used for the computation of Crit(θ). During the parameter optimization procedure, the experimental and simulated data of the six experiments were concatenated in order to reduce the risk of convergence towards a local minimum.

3. The dissolution rate constant K_d defined in Eq. 13 was easily estimated through the separate identification of a

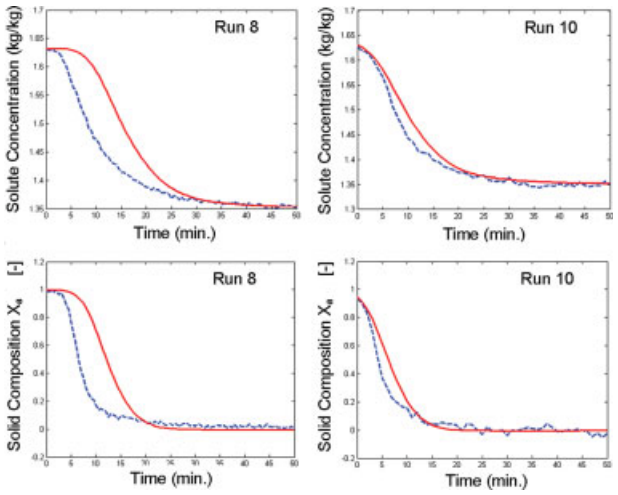

Figure 11. Comparison between simulated (full lines) and experimental (dashed lines) solute concentration profiles and "pseudo-polymorphic" composition during Runs 8 and 10, performed with similar initial supersaturation and 0.1 and 10 g of mCA seed particles, respectively.

[Color figure can be viewed in the online issue, which is available at www.interscience.wiley.com.]

specific aCA dissolution run monitored using in situ Raman spectroscopy.[22]

The five kinetic parameter values required to solve Eqs. 4–13 were thus estimated prior to the present study. Now, based on the kinetic expressions (11–13), the phase transition experiments were simulated and compared with the experimental results obtained during Runs 8–12 presented in Table 1. It is worthy of noting that the parameters used to simulate the aCA to mCA transition process were therefore obtained from experiments performed in the absence of any phase transition process. As far as the consistency of the parameter estimates of the SMPT process is concerned, it is reasonable to assume that such precautionary procedure reinforces the whole modeling and identification scheme.

The SMPT simulations are partly presented in Figure 11. For the sequel, it is important to keep in mind that the observed model-experiment mismatches increase with decreasing seed amounts (see Table 1). Indeed, it is clear that the kinetic Eqs. 11–13 are such that the overall model-predicted rate of turnover should increase with the amount of stable seeds, which contradicts the experimental observations. Moreover, the simulated rate of turnover is underestimated with respect to the real one, especially when low seed amounts were used.

On the one hand, the kinetics of mCA growth and aCA dissolution characterized previously should not be changed by the occurrence of the crystallization of the stable form. On the other hand, the experimental results of mCA crystallization operations performed in the absence of metastable aCA particles have clearly shown that the nucleation of mCA was depending on the concentration of mCA in suspension. The generation of new particles could therefore result from aCA interparticles impacts or birth of stable particles on aCA surfaces. Anyway, in both cases, the metastable solid content is expected to play a role in the nucleation process. This is the reason why it appeared logical to account also for the concentration of metastable solid in the rate of secondary mCA nucleation, even though the respective effect of the two different forms was not expected to exhibit the same supersaturation- and solid concentration-dependence. The following secondary nucleation rate Eq. 17 was thus set, where the new parameter α was introduced so as to account for possible differences between nucleation of stable crystals due to the presence of stable or metastable particles:

$$R_{N_{2m}}(t) = 1.72 \times 10^8 \left[C_{S,m}(t) + \alpha\, C_{S,a}(t)\right]^{0.47} (C(t) - C_m^*)^{1.14} \tag{17}$$

where $C_{S,a}$ is the concentration of monohydrate crystals in suspension [kg/m^3].

A priori, and as far as the contribution of $C_{S,a}$ and $C_{S,m}$ in the rate of nucleation of the stable form is concerned, exponents i_m and j_m and parameter K_{2m} defined by Eq. 12 are not expected to be identical. However, Eq. 17 was set as a first approximation in order not to increase too much the number of kinetic parameters to estimate. Equation 17 was applied to the seeded SMTP experiments, and the identification strategy described by Caillet et al.[23] was then run to estimate the value of α minimizing the mismatch between the simulated and the experimental data.

Discrete time experimental CSD data could not be used here to estimate parameter α. This is firstly because the initial amount of aCA solid particles does not allow any size measurements using image analysis. Secondly, the shape of citric acid particles does not allow distinguishing between monohydrate and anhydrous crystals. However, unlike the estimation of θ, two continuous measurements are now available through Raman spectroscopy[19]: supersaturation and solid composition data provide a reasonable amount of data for computing the model/experiment quadratic prediction errors.

Surprisingly, the optimal value of α was finally found to be almost equal to 1 (i.e., α optimal $\approx$1.06). A really satisfactory representation of the experimental results was thus obtained as one can see in Figure 12. Finally, the secondary nucleation rate of mCA particles was therefore set as follows:

$$\begin{aligned} R_{N_{2m}}(t) &= 1.72 \times 10^8 \left[C_{S,m}(t) + 1.06\, C_{S,a}(t)\right]^{0.47} (C(t) - C_m^*)^{1.14} \\ &\cong 1.72 \times 10^8\, C_{S,T}(t)^{0.47} (C(t) - C_m^*)^{1.14} \end{aligned} \tag{18}$$

where $C_{S,T}$ is the overall solid concentration.

Clearly, $\alpha = 1$ means that the secondary nucleation rate of stable particles on contact with metastable or stable crystals is equal in both cases: as outlined above this feature of secondary nucleation was rather unexpected. It is also worthy of noting that Eq. 18 explains the specific kinetic features of the phase transition process underlined previously and, in particular, the experimental fact that the initial rate of generation of new stable particles is not changed by the amount of seed particles.

As an example of the Femlab simulation of the CSD evolutions during the SMPT process, Figure 13 displays the plots of the time variations of both aCA and mCA CSD

during Run 9. As one can see, the metastable particles are almost fully dissolved after about 750 s and the last percent of solid vanishes around time $t \approx 1000$ s. The logarithmic size axis shows that the increase of the number of new stable particles, through secondary nucleation, is almost exponential until the end of the batch process.

Conclusion

The "pseudo-polymorphic" SMPT of citric acid in water, from the anhydrous to the monohydrate form, was investigated at 15 C. The process was satisfactorily described through PBEs based on growth, dissolution, and nucleation kinetic expressions, enabling previous and present experimental results to be described. A set of kinetic parameters was estimated after minimizing the difference between the measured solute and solid-phase concentrations, together with the difference between off-line infrequent CSD data and their model-predicted values. The kinetic parameters were partly estimated after previously reported studies.[21–23]

The overall SMPT kinetic scheme was shown to be consistent with the rather rare experimental results available in the open literature. This in turns confirms that one can mathematically describe complex SMPT kinetic processes using "standard" kinetic data and models. However, a cautious analysis of both experimental and modeling results obtained after the investigation of various model polymorphic systems (i.e., 2,6DHB acid, L-Glutamic acid, Glycine) revealed that understanding and predicting the nucleation of stable forms in the presence of metastable ones remains an open issue in the development of predictive SMTP kinetic models.

From this latter point of view, it was found here that the nucleation of stable monohydrate Citric Acid (mCA) in the presence of the metastable anhydrous form (aCA) was governed by the same kinetic law and the same kinetic parameters than the secondary nucleation of aCA, which is a rather surprising result. Indeed, on the one hand, it was experimentally observed that no nucleation of stable form was occurring in the presence of metastable seed particles. On the other hand, whatever the amount of stable seed introduced in the steady-state slurry, subsequent nucleation of stable form is essentially depending on the metastable solid content through a supersaturation dependent kinetic mechanism. This interesting feature of the nucleation process, and the corresponding physical mechanisms involved, will have to be investigated more deeply in future studies.

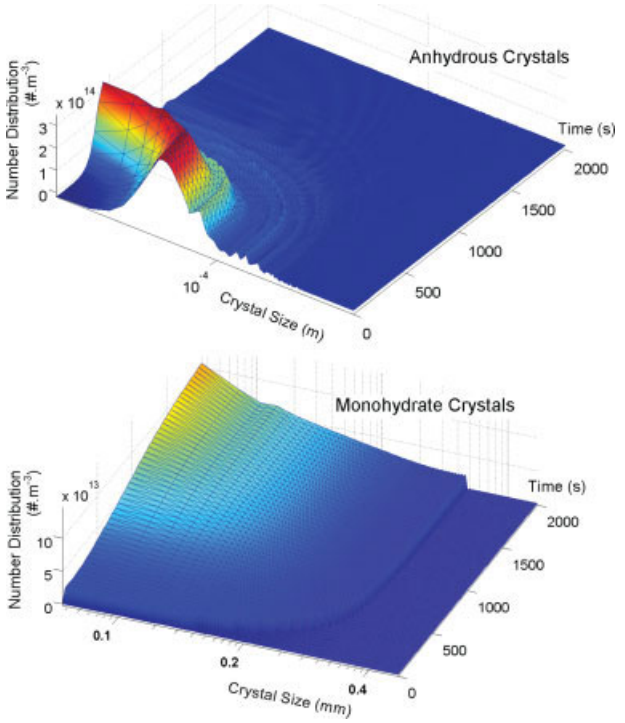

Figure 13. Simulated CSD profiles for anhydrous and monohydrate Citric Acid crystals during the isothermal phase transition at 15 C (Run 9).

The nucleation rate was expressed by Eq. 18 with $\alpha = 1$. [Color figure can be viewed in the online issue, which is available at www.interscience.wiley.com.]

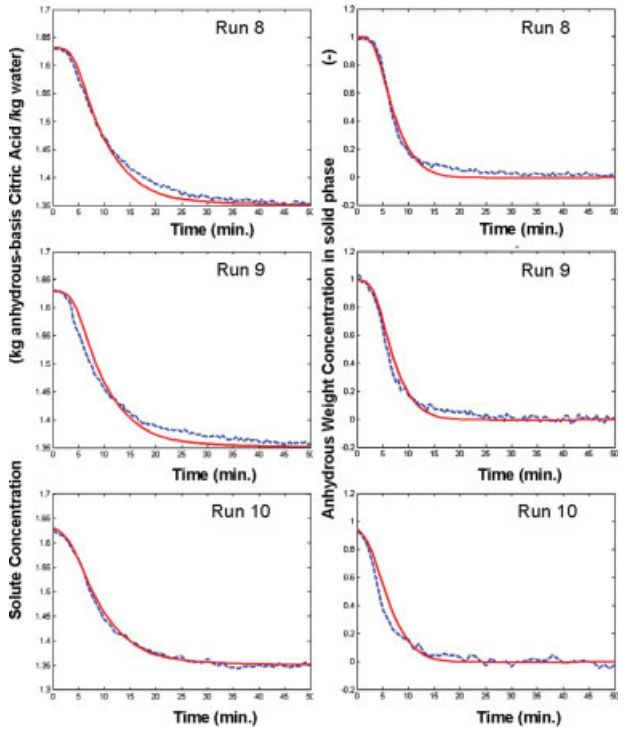

Figure 12. Comparison between simulated (full lines) and experimental (Dashed lines) solute concentration profiles and "pseudo-polymorphic" composition during Runs 8–10.

The nucleation rate was expressed by Eq. 18 with $\alpha = 1$. [Color figure can be viewed in the online issue, which is available at www.interscience.wiley.com.]

Literature Cited

1. Ostwald W. Studien über die bildung und umwandlung fester körper. *Zeitschrift für Physikalische*. 1897;22:289–330.
2. Bernstein J. Crystal growth, polymorphism and structure-property relationships in organic crystals. *J Phys D: Appl Phys*. 1993;26: B66–B76.

3. Brittain HG. *Polymorphism in Pharmaceutical Solids*. New York: Marcel Dekker, 1999.
4. Bernstein J, Henck JO. Disappearing and reappearing polymorphs—an anathema to crystal engineering? *Cryst Eng*. 1998;1:119–128.
5. Threlfall TL. Analysis of organic polymorphs. A review. *Analyst (Cambridge, UK)*. 1995;120:2435–2460.
6. Giron D. Thermal analysis and calorimetric methods in the characterization of polymorphs and solvates. *Thermochim Acta*. 1995;248: 1–59.
7. Yu L, Reutzel SM, Stephenson GA. Physical characterization of polymorphic drugs: an integrated characterization strategy. *Pharm Sci Technol Today*. 1998;1:118–127.
8. Center for Drug Evaluation and Research, Office of Training and Communication, Division of Drug Information. PAT—a framework for innovative pharmaceutical development, manufacturing and quality assurance. FDA Guidance for Industry. Rockville, MD: Center for Drug Evaluation and Research, 2004. HFD-240.
9. Auer ME, Griesser UJ, Sawatzki J. Qualitative and quantitative study of polymorphic forms in drug formulations by near infrared FT-Raman spectroscopy. *J Mol Struct*. 2003;661/662:307–317.
10. Cardew PT, Davey RJ. The kinetics of solvent-mediated phase transformations. *Proc R Soc London Ser A: Math Phys Eng Sci*. 1985; 398:415–428.
11. Ono T, ter Horst JH, Jansens PJ. Quantitative measurement of the polymorphic transformation of L-glutamic acid using in-situ Raman spectroscopy. *Cryst Growth Des*. 2004;4:465–469.
12. Ono T, Kramer HJM, ter Horst JH, Jansens PJ. Process modeling of the polymorphic transformation of L-glutamic acid. *Cryst Growth Des*. 2004;4:1161–1167.
13. Starbuck C, Spartalis A, Wai L, Wang J, Fernandez P, Lindemann CM, Zhou GX, Ge Z. Process optimization of complex pharmaceutical polymorphic system via in situ Raman spectroscopy. *Cryst Growth Des*. 2002;2:515–522.
14. Wang F, Wachter JA, Antosz FJ, Berglund KA. An investigation of solvent-mediated polymorphic transformation of progesterone using in situ Raman spectroscopy. *Org Process Res Dev*. 2000;4: 391–395.
15. Schöll J, Bonalumi D, Vicum L, Mazzotti M, Muller M. In situ monitoring and modeling of the solvent-mediated polymorphic transformation of L-glutamic acid. *Cryst Growth Des*. 2006;6:881–891.
16. Agarwal P, Berglund KA. In situ monitoring of calcium carbonate polymorphs during batch crystallization in the presence of polymeric additives using raman spectroscopy. *Cryst Growth Des*. 2003;3:941–946.
17. Hu YR, Liang JK, Myerson AS, Taylor LS. Crystallization monitoring by Raman spectroscopy: simultaneous measurement of desupersaturation profile and polymorphic form in flufenamic acid systems. *Ind Eng Chem Res*. 2005;44:1233–1240.
18. Qu H, Louhi-Kultanen M, Rantanen J, Kallas J. Solvent-mediated phase transformation kinetics of an anhydrate/hydrate system. *Cryst Growth Des*. 2006;6:2053–2060.
19. Schöll J, Vicum L, Müller M, Mazzotti M. Precipitation of L-glutamic acid: determination of nucleation kinetics. *Chem Eng Technol*. 2006;29:257–264.
20. Schöll J. *Nucleation, Growth and Solid Phase Transformation During Precipitation Processes*, PhD Dissertation. Zurich: Swiss Federal Institute of Technology (ETH), 2006.
21. Caillet A, Puel F, Fevotte G. In-line monitoring of partial and overall solid concentration during solvent-mediated phase transition using Raman spectroscopy. *Int J Pharm*. 2006;307:201–208.
22. Caillet A, Rivoire A, Galvan JM, Puel F, Févotte G. Crystallization of monohydrate citric acid, Part 1: in situ monitoring through the joint use of Raman spectroscopy and image analysis. *Cryst Growth Des*. In press.
23. Caillet A, Sheibat-Othman N, Févotte G. Crystallization of monohydrate citric acid, Part 2: modeling through population balance equations. *Cryst Growth Des*. In press.
24. Lorenz H, Perlberg A, Sapoundjiev D, Elsner MP, Seidel-Morgenstern A. Crystallization of enantiomers. *Chem Eng Process* (Particulate Process: Spec Issue). 2006;45:863–873.
25. Elsner MP, Fernandez Menendez D, Alonso Muslera E, Seidel-Morgenstern A. Experimental study and simplified mathematical description of preferential crystallization. *Chirality*. 2005;17:183–195.
26. Davey RJ, Blagden N, Righini S, Alison H, Quayle MJ, Fuller S. Crystal polymorphism as a probe for molecular self-assembly during nucleation from solutions: the case of 2,6-dihydroxybenzoic acid. *Cryst Growth Des*. 2001;1:59–65.
27. Davey RJ, Blagden N, Righini S, Alison H, Ferrari ES. Nucleation control in solution mediated phase transformations: the case of 2,6-dihydroxybenzoic acid. *J Phys Chem B*. 2002;106:1954–1959.
28. Ferrari ES, Davey RJ. Solution-Mediated transformation of α to β L-glutamic acid: rate enhancement due to secondary nucleation. *Cryst Growth Des*. 2004;4:1061–1068.
29. Cashell C, Corcoran C, Hodnett BK. Secondary nucleation of the β-polymorph of L-glutamic acid on the surface of α-form crystals. *Chem Commun*. 2003;3:374–375.
30. Ferrari ES, Davey RJ, Cross WI, Gillon AL, Towler CS. Crystallization in polymorphic systems: the solution-mediated transformation of β to α glycine. *Cryst Growth Des*. 2003;3:53–60.
31. Groen H, Roberts KJ. Nucleation, growth, and pseudo-polymorphic behavior of citric acid as monitored in situ by attenuated total reflection fourier transform infrared spectroscopy. *J Phys Chem B*. 2001; 105:10723–10730.
32. Ramkrishna D. *Population Balances*. London: Academic Press, 2000.

Manuscript received Jan. 9, 2007, and revision received May 25, 2007.